Margaret Antonik
Mechanical and Aerospace Engineering,
North Carolina State University,
911 Oval Drive,
Raleigh, NC 27695
e-mail: mrantoni@ncsu.edu

Brendan T. O'Connor
Assistant Professor
Mechanical and Aerospace Engineering,
North Carolina State University,
911 Oval Drive,
Raleigh, NC 27695
e-mail: btoconno@ncsu.edu

Scott Ferguson
Associate Professor
Mechanical and Aerospace Engineering,
North Carolina State University,
911 Oval Drive,
Raleigh, NC 27695
e-mail: scott_ferguson@ncsu.edu

Performance and Design Comparison of a Bulk Thermoelectric Cooler With a Hybrid Architecture

This paper compares the economic viability and performance outcomes of two different thermoelectric device architectures to determine the advantages and appropriate use of each configuration. Hybrid thermoelectric coolers (TECs) employ thin-film thermoelectric materials sandwiched between a plastic substrate and form a corrugated structure. Roll-to-roll (R2R) manufacturing and low-cost polymer materials offer a cost advantage to the hybrid architecture at the sacrifice of performance capabilities while conventional bulk devices offer increased performance at a higher cost. Performance characteristics and cost information are developed for both hybrid and conventional bulk single-stage thermoelectric modules. The design variables include device geometry, electrical current input, and thermoelectric material type. The tradeoffs between cooling performance and cost will be explored, and the thermoelectric system configuration is analyzed for both hybrid and conventional bulk TECs. [DOI: 10.1115/1.4032637]

1 Introduction

Thermoelectric (TE) modules are quiet, reliable, and scalable solid-state devices that use TE materials to (1) convert waste heat to energy via the Seebeck effect or (2) convert energy to cooling or heating via the Peltier effect [1]. TECs may be a particularly attractive alternative to traditional refrigeration systems because they eliminate the use of ozone-depleting and greenhouse-gas emitting hydrofluorocarbon refrigerants. Further, the durability and reliability of TECs have led to diverse applications that include commercial products, military purposes, aerospace uses, scientific and medical equipment, microelectronics, and solar-driven thermoelectric cooling devices [2].

Initial applications of TECs have led to reduced fuel consumption in hybrid vehicles [3], increased control of microprocessor chip temperatures [3,4], and reduced fossil power usage when used as heat pumps [5]. While the advantages of thermoelectric technology are promising, a major drawback preventing widespread adoption is their inefficiency leading to high operating costs. To work beyond niche applications of TECs, a better understanding of the performance and design space of a TEC is needed to drive future development.

This work explores a hybrid architecture that combines a conventional bulk device with an in-plane thin-film device. A bulk device has TE material deposited on a substrate in thicknesses on the order of millimeters; in contrast, thin-film deposits on a substrate are microns thick. This leads to a challenge of maintaining a temperature differential across the device. While taking advantage of low-cost R2R manufacturing to print thin-film layers of TE material on a substrate, the hybrid architecture is able to maintain a cross-plane heat flux like in a bulk device [6,7].

Analysis is needed that explores how the geometric factors, heat exchanger options, device architecture, TE material, and operating power influence the cooling performance and efficiency of a TEC and overall system costs. Toward this goal, this paper extends an existing cost metric and expands the performance equations for TEC analysis [1,8–10]. Additional performance considerations include a heat exchanger and spreading resistance. Unlike previous analyses of TECs, this study considers multiple objectives, additional design variables and model considerations, a heat exchanger on the hot side of the TEC, and multiple TE materials. Furthermore, both bulk and hybrid device architectures are compared. Exploring the economic and performance characteristics of a TEC manufactured via screen-printing techniques offers insights into the viability of R2R manufacturing's applicability to TE devices. Additionally, materials with improved thermoelectric figures of merit are explored, and system costs are decomposed to identify major contributions to the overall cost of a TEC. Through identification of heat exchanger, substrate, and TE material costs and the impact of increased TE material efficiency, a more complete understanding of the potential for TECs to reach wider adoption is realized.

2 Background

Theoretical advances in areas of electron and phonon transport have led to a renewed focus on thermoelectrics as a green technology [11], as nanostructured and complex bulk materials allow for efficiencies capable of competing with other cooling technologies [12]. ZT, given in Eq. (1), is the figure of merit providing a metric for the efficiency limit of a TE material

$$\mathrm{ZT} = \frac{\alpha^2}{\kappa\rho} T \tag{1}$$

Maximizing ZT requires a large Seebeck coefficient (α), low thermal conductivity (κ), and low electrical resistivity (ρ). To improve the efficiency of thermoelectric devices, a designer must navigate the tradeoffs that occur when developing high-performance materials. Improving the figure of merit of a material [1] requires navigating the conflicting goals of increasing the Seebeck coefficient, decreasing thermal conductivity, and increasing electrical conductivity. Environmentally friendly and stable polymer TE materials offer printable solutions that can be used in R2R manufacturing on flexible substrates [13]. In comparison to current inorganic materials like BiTe with ZT up to $\sim$2.2, the best reported ZT value for polymer TE material poly(3, 4-ethylenedioxythiophene):poly(styrenesulfonate) (PEDOT:PSS) is 0.4 [14,15].

Additionally, novel architectures for large-scale devices may be needed to maintain an appropriate heat flow. Designers must

Contributed by the Heat Transfer Division of ASME for publication in the Journal of Thermal Science and Engineering Applications. Manuscript received August 11, 2015; final manuscript received December 18, 2015; published online March 1, 2016. Assoc. Editor: Samuel Sami.

consider device configuration, TE materials, manufacturing costs, operating conditions and temperatures, heat exchangers, cooling requirements, and efficiency requirements. Previous thermoelectric design and optimization research has focused on cooling capacity (Q_C) and coefficient of performance (COP). Yamanashi used dimensionless quantities to analyze the linkage between thermoelectric properties and heat exchanger design [16]. It was found that the hot-side heat exchanger has a greater performance effect than the cold side heat exchanger. Huang et al. used performance curves of actual TEC modules to analyze maximum COP and maximum Q_C designs [17], while Cheng and Lin used a genetic algorithm (GA) to maximize Q_C in a confined volume while treating COP and cost—calculated using TE material costs—as constraints [18]. Later work considered the multiobjective analysis of two-stage TECs [19].

GAs were used by Nain et al. to show that the structural parameters of the TE elements (leg length and area) have significant influence on COP and Q_C [20]. Zhou and Yu maximized COP and Q_C separately by allocating thermal conductance of hot and cold heat exchangers [21]. Huang et al. used the simplified conjugate gradient method to optimize geometric structure for maximum Q_C with a constraint on COP and found that leg length should be as small as possible and area of the TE legs as large as possible [22]. Venkata Rao and Patel implemented a modified teaching–learning based optimization algorithm to maximize a weighted sum objective combining COP and Q_C for two-stage TECs [23]. Finally, research by Khanh et al. tested the effectiveness of GAs and simulated annealing for single-stage TECs and indicated in a preliminary conclusion that simulated annealing was more robust [24].

Rather than focusing solely on performance, other works have explored TECs and thermoelectric generators (TEGs) with a focus on cost performance [8,10,25]. While considering the cost/efficiency tradeoffs of a TEG, the results in Ref. [26] indicated that polymer materials could prove advantageous in application. Yee et al. introduced a cost per unit of power (\$/W) cost metric (considering material, manufacturing, and heat exchanger costs) for TEGs and optimized the TE leg length and system fill factor for the minimum \$/W [25]. This work demonstrated how expensive TE materials could be cost effective in a TEG system if implemented with short TE legs and small fill factors. LeBlanc et al. built on these efforts by analyzing additional TE materials and introducing a cost metric (\$/kWh) for TECs [8].

These metrics provide the basis for the cost analysis completed in this study, and prior optimization efforts provide a foundation for exploring how a new device architecture can help to realize the potential of TECs. While LeBlanc et al. introduced the cost metric for TECs, their work did not include heat exchangers in the overall system cost [8]. Works that included heat exchangers and spreading resistance only considered cost as thermoelectric material cost, ignoring additional manufacturing costs. These limitations, under the context of thermoelectric materials and alternative device architectures, provide a motivation for the steps taken in this work. In Sec. 3, the standard set of equations for a TEC will be introduced, and the additional model considerations of spreading resistance and heat exchangers will be discussed.

3 Modeling the TECs

The hybrid architecture studied in this work maintains a cross-plane heat flux across the p-type and n-type legs. If the device is constructed using R2R processing, the TE materials can be rotary screen printed on a flexible plastic (polyethylene terephthalate (PET)) substrate in thicknesses of 50–250 μm, with a leg width over 10 mm and a leg length between 10 and 20 mm [27]. This allows for larger temperature differences across the TE legs than other thin-film devices where leg lengths are smaller than a few hundred microns. The unit equipment cost of a rotary screen printer is approximately \$73,000 if a 250 mm print width is desired along with an ink pump and ink level control unit to maintain a constant, consistent ink level [28].

Figure 1(a) depicts the printing pattern of the material on the PET substrate. A silver paste ink can be used to create the metal interconnects [12]. After printing on one layer of PET substrate, the TE layer is laminated with two more PET layers to sandwich the legs. The module is then processed to shape the device in a way that maintains the cross-plane heat flux like a bulk device. The final device configurations for a hybrid TEC and a bulk TEC are given in Figs. 1(b) and 1(c), respectively. The process presented here is hypothetical, but the approach is supported by prior work in Refs. [6,13,29], and [30].

Figure 2 provides a diagram of a TEC system and the equivalent thermal resistance circuit model. Heat balance between Q_C and Q_H provides the foundation for the standard analytical model of a TEC with power input P. Thermal resistance is a function of the heat exchanger (R_{HX}), the thermoelectric elements (R_{TE}), and the spreading resistance from the substrate (R_{spread}).

TE legs only occupy a fraction of the substrate's footprint. The fill factor is defined as the cross-sectional area of the TE legs divided by the cross-sectional area of the device. This number is bounded between 0 and 1. Small fill factors reduce the heat flow across the device; thus, to work toward a more accurate model, thermal spreading resistance needs to be accounted for Ref. [10]. However, we do not consider the thermal resistance of air when the fill factor is very small.

To calculate spreading resistance, steps must be taken to convert the rectangular areas of the TE legs (A_{TE}) and the device (A) to a circular geometry, as given by Eqs. (2) and (3).

$$a = \sqrt{\frac{A_{\mathrm{TE}}/2}{\pi}} \tag{2}$$

$$b = \sqrt{\frac{A/2}{\pi}} \tag{3}$$

Dimensionless solutions for contact radius (ε) and plate thickness (τ) are then determined using Eqs. (4) and (5) to simplify the presentation of solutions [9].

$$\varepsilon = \frac{a}{b} \tag{4}$$

$$\tau = \frac{d_s}{b} \tag{5}$$

An empirical parameter (λ_c) is calculated followed by a dimensionless parameter (Φ_c) and dimensionless constriction resistance (ψ). These three equations represent a simple approximation, noted to be in agreement with numerical solutions, to analytical solutions developed by Song et al. [9] and are given by Eqs. (6)–(8). Finally, the spreading resistance (R_{spread}) is determined by Eq. (9), where κ_s is the thermal conductivity, d_s is the thickness, and Bi is the Biot number of the film supporting the TE materials. The Biot number is set to 0.1 under the assumption that the temperature gradient inside the substrate is negligible.

$$\lambda_c = \pi + \frac{1}{\sqrt{\pi}\varepsilon} \tag{6}$$

$$\Phi_c = \frac{\tanh(\lambda_c\tau) + \dfrac{\lambda_c}{\mathrm{Bi}}}{1 + \dfrac{\lambda_c}{\mathrm{Bi}}\tanh(\lambda_c\tau)} \tag{7}$$

$$\psi = \frac{\varepsilon\tau}{\sqrt{\pi}} + 0.5(1-\varepsilon)^{3/2}\Phi_c \tag{8}$$

$$R_{\mathrm{spread}} = \frac{\psi}{\sqrt{\pi}}\kappa_s a \tag{9}$$

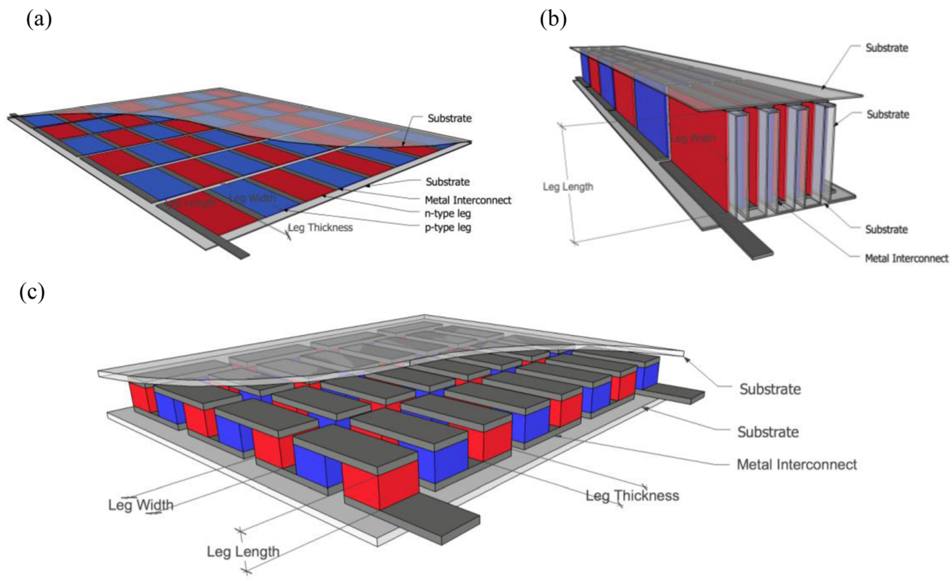

Fig. 1 Illustrations of (*a*) printing pattern of material on substrate, (*b*) hybrid TEC after processing into final form, and (*c*) bulk TEC

The thermal resistance through the TE legs, R_{TE}, is given in Eq. (10). The electrical resistance (R), total thermal conductance (K), and Seebeck coefficient (α) are given in Eqs. (11)–(13). In these equations, t, w, and L are leg thickness, width (tw is the cross-sectional area of the TE leg), and length, respectively. The properties of the p-type and n-type legs (designated by the subscripts p and n) comprise the total material properties: κ represents the material thermal conductivity, ρ the electrical conductivity, and α the Seebeck coefficient.

$$R_{\mathrm{TE}} = \frac{1}{(\kappa_p + \kappa_n)\frac{tw}{L}} \tag{10}$$

$$R = (\rho_p + \rho_n)\frac{L}{tw} \tag{11}$$

$$K = \frac{1}{R_{\mathrm{TE}} + R_{\mathrm{spread}}} \tag{12}$$

$$\alpha = \alpha_p - \alpha_n \tag{13}$$

Cooling using a TEC must overcome Joule heating and the heat conduction through the TEC legs. Half of the Joule heating flows to each of the junctions of the TEC. Combining the Peltier effect, Joule heating, and the Fourier effect, the heat absorption into the device, Q_C, is given in Eq. (14). Joule heating is designated by the term $(1/2)I^2R$, the Fourier effect is described by $K(T_H - T_C)$, and the Peltier effect by $I\alpha T_C$. Similar to the heat absorption on the cold side of the device (Q_C), the energy balance equations give the heat rejected at the hot side (Q_H), given in Eq. (15). The heat conduction through the legs is between the junction temperatures T_H and T_C. The power input, P is shown in Eq. (16). An energy balance of the system gives $P = Q_H - Q_C$. In these equations, N is the number of thermocouples, and I is the input current

$$Q_C = N\left[I\alpha T_C - K(T_H - T_C) - \frac{1}{2}I^2R\right] \tag{14}$$

$$Q_H = N\left[I\alpha T_H - K(T_H - T_C) + \frac{1}{2}I^2R\right] \tag{15}$$

$$P = N[I\alpha(T_H - T_C) + I^2R] \tag{16}$$

To simplify the analytical model, a common assumption is to consider the heat sink only on the hot side [24]. An infinite sink is assumed on the cold side, and the known ambient air temperature (T_∞) along with the overall heat transfer coefficient (U) and cross-sectional area of the device is used to determine the hot-side junction temperature (T_H), calculated by Eq. (17)

$$T_H = Q_H\frac{1}{UA} + T_\infty \tag{17}$$

Finally, the COP, Eq. (18), is given by the heat absorbed by the device divided by the power expenditure into the device.

$$\mathrm{COP} = \frac{Q_C}{P} \tag{18}$$

Several common assumptions are made in the development of this analytical model [1]. The p-type and n-type TE elements have the same basic geometries, rectangular shapes sharing the same leg length, thickness, and width. The Seebeck coefficient, thermal conductivity, and electrical resistivity of the TE material are considered temperature independent [31]. For simplicity, the thermal and electrical contact resistances of the thermal interface layer and the metal are treated as negligible, and the Thomson effect is neglected [1]. The Thomson effect can be neglected because it has been shown that, for a wide range of temperatures, models incorporating the Thomson effect show close agreement with the standard set of TE equations [32]. Additionally, the TE material substrate in the hybrid device is neglected, where it has previously been shown to be a minor parasitic loss when the TE materials are much thicker than the substrate [7], which is the case here.

4 Device Cost Metric

The cost breakdown for a TEC and the parameters that contribute to the cost are given in Fig. 3. The cost metric analysis is derived from the work in Refs. [8] and [25]. A contribution of this paper is to incorporate heat exchangers into the analysis of a TEC by using a similar procedure as that for TEGs. The total cost of a TEC can be subdivided into operating cost and capital cost. The operating cost considers the efficiency of a device through its COP and the cost of the power source. Capital cost can be broken into three segments: TE material, substrate, and heat exchanger. This cost metric is measured by $/kWh of cooling.

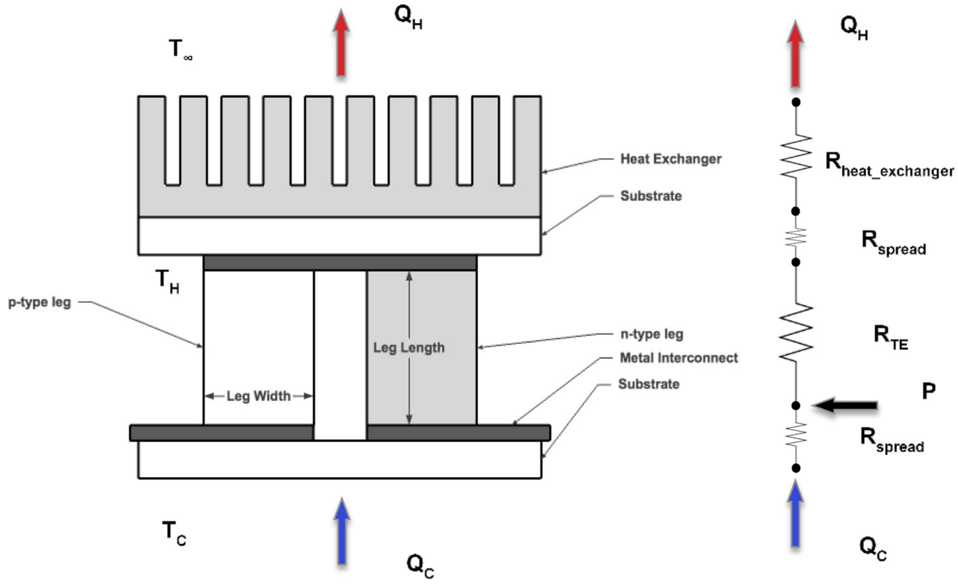

Fig. 2 Basic diagram of a TEC and the equivalent thermal resistance circuit of the system

Device geometry and material, manufacturing, and heat exchanger costs are considered key components in a cost metric for a TE. Yee et al. presented a cost metric that includes these components while incorporating volumetric material costs (C'''), areal material costs (C''), and heat exchanger/ceramic substrate costs (C_{HX}) [25]. Volumetric and areal costs were determined by considering equipment prices (for ball milling, melt spinning, spark plasma sintering, dicing, metallization, microfabrication, and screen printing) and heat exchanger costs were derived from actual engineering data on heat exchangers compiled in Ref. [33]. To analyze the total system cost of a TEC and to study the bulk and hybrid architectures, which have different substrate materials, the heat exchanger/substrate component of the cost metric in Ref. [25] is separated into heat exchanger cost and substrate cost (C_s). This allows for a deeper analysis of the effects of the heat exchanger on system cost and for the use of different substrate materials (ceramic for the bulk device and PET for the hybrid device). Using the volumetric (C'''), areal (C''), heat exchanger (C_{HX}), and substrate cost (C_s) components, the overall system cost (C) of a TEC is given in Eq. (19). An operating cost, in terms of \$/hr, based on the cost of electricity (C_e) and power input into a device (P) is given in Eq. (20).

$$C_{\mathrm{capital}} = N[(C'''L + C'')wt + C_{\mathrm{HX}}UA + C_sA] \tag{19}$$

$$C_{\mathrm{operating}} = C_eP \tag{20}$$

LeBlanc et al. extended this basic capital cost metric by providing a list of common TE materials [8]. These manufacturing costs are an appropriate lower bound for the estimated costs of manufacturing the thermoelectric material [8,34]. The volumetric material costs (C''') include the cost of the thermoelectric material on a \$/kg basis and volumetric manufacturing costs like ball milling and hot pressing. The areal material costs (C'') include the cost of metallization and areal manufacturing costs, such as dicing and cutting.

These costs are associated with the price of the equipment used in manufacturing and the quantity of TE devices processed on that equipment. The cost of equipment, which is given in Table 1, and material cost were gathered from raw material costs reported in the *U.S. Geological Survey* [8]. In addition, Leblanc et al. derived heat exchanger costs using data in Refs. [33] and [35]. The heat exchanger cost is scaled with the overall heat transfer coefficient and given in \$/(W/K) and is closely related to the heat transfer coefficient of the exchanger.

COP is considered to calculate an operating cost. Continuous operation over a 20-year period (the industry standard for the mean time between failures is over 200,000 hrs) is used, so the amortized cost can be simplified. This cost metric, developed in Ref. [8] and given in Eq. (21), is expressed in \$/kWh and includes the capital cost amortized over the lifetime and the lifetime operating cost for a given cooling capacity. In this equation, r is the amortization rate

$$H = \frac{C_{\mathrm{operating}}}{Q_C} + r\frac{C_{\mathrm{capital}}}{\mathrm{COP}\cdot P} \tag{21}$$

5 Optimization Problem Formulation

This section describes the optimization problems formulated to explore the performance and design spaces of bulk and hybrid TECs. Several formulations are considered: (1) a multiobjective

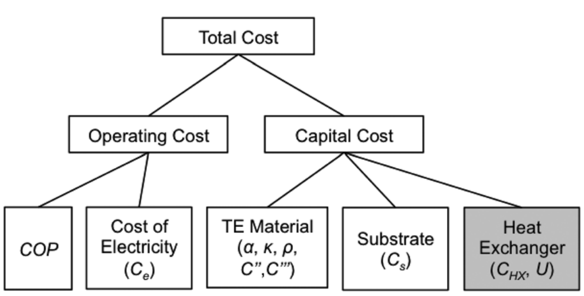

Fig. 3 Breakdown of the total cost of a TEC system

Table 1 Manufacturing process and associated equipment cost (adapted from Ref. [8])

	Process	Equipment cost (\$)
Volumetric processing	Ball milling	40,000
	Melt spinning	135,000
	Spark plasma sintering	400,000
Areal processing	Dicing	150,000
	Metallization	200,000
	Molecular beam epitaxy	600,000
	Screen printing	50,000

problem [36] with the goals of minimizing cost and maximizing cooling capacity, (2) a single objective problem with the goal of minimizing the device area for a given cooling capacity, and (3) two single objective problems that minimize capital cost and operating cost.

Bounds for the optimization of a bulk TEC are set by manufacturing constraints and those established in the literature [1,2,18,24]. Twenty-five material choices were investigated, and their properties are listed in Table 7. Side constraints for the hybrid architecture were also determined to reflect geometry changes, the different TE materials allowed, and the manufacturing considerations for screen-printed inks and processing of the PET substrate [8,13,29,37]. Two material choices were available for the hybrid architecture. A BiTe-polymer composite printable material can be used, and PEDOT:PSS material properties are updated to reflect the results from Bubnova et al. [14]. To use BiTe as a printable solution, BiTe is mixed with polymer binders and solvents—the result is a composite TE material with a ZT value of 0.18 [29]. Side constraints for each design variable are tabulated in Table 2.

Operating temperatures are set to an ambient temperature of 20 °C with the cold side temperature at 0 °C. Alumina ceramic is the substrate for the bulk device [1]. PET plastic is the substrate for the hybrid architecture [37]. Table 3 details the properties and design parameters found in the fundamental TE equations and the cost model.

5.1 Multiobjective Problem Formulation.

It is expected that the hybrid architecture will be better suited to low cooling density applications but will require a larger footprint. This is because it is inexpensive to scale the design up in size, but solutions are also limited to low ZT thermoelectric materials. A multiobjective problem can be formulated as shown in Eq. (22) with the goals of finding the optimal device parameters that maximize cooling capacity, Q_C from Eq. (14), and minimize the total device cost, H from Eq. (21).

$$\begin{aligned} \text{Minimize:}\quad & f_1 = -Q_C \\ & f_2 = H \\ \text{Subject to:}\quad & \text{Side bounds established for each architecture} \end{aligned} \tag{22}$$

As a population-based approach, NSGA-II is well suited to this multiobjective problem [42]. The size of the population at each generation was set to 90 designs, ten times the number of design variables. Tournament selection was used with four candidates, and a scattered crossover operator was used with a 0.5 crossover rate. A uniform mutation operator was used with a 5% chance of mutation. The algorithm terminated after 100 generations, and a hypercube measurement was used to measure convergence.

5.2 Single Objective Problem Formulations.

From the multiobjective optimization results that will be introduced in Sec. 6.1, BiSbTE nanobulk for the bulk device and the PEDOT:PSS material for the hybrid device are the lowest cost and highest performing materials. This allows material choice to be removed as a design variable. To explore the problem further, an initial hypothesis was that the hybrid device would require a larger number of thermocouples and a much larger area to produce the same amount of cooling as a bulk device. This hypothesis was formulated because the bulk TEG will have more active thermoelectric material per unit area than the hybrid device. To help determine the area requirement differences for the bulk and the hybrid architectures when the cooling capacity, desired operating temperatures, and allowable cross-sectional area are known, a single objective optimization problem is formulated to minimize the cross-sectional area for a given Q_C. The objective in Eq. (23) minimizes cross-sectional area of the device with two inequality constraints to maintain the Q_C within ± 5% of a target Q_C value (y). The GA function in MATLAB is used with default settings to solve for optimal solutions [43].

$$\begin{aligned} \text{Minimize:}\quad & f = A_{\text{total}} = AN \\ \text{Subject to:}\quad & Q_C - 1.05y \le 0 \\ & 0.95y - Q_C \le 0 \\ & \text{Side bounds established for each architecture} \end{aligned} \tag{23}$$

To provide a more detailed analysis of cost drivers, H can also be decomposed into operating cost and capital cost. In Refs. [10] and [18] just the cost of TE material was considered, making the cost dependent only on the volume of the material used. When incorporating the cost of a heat exchanger, minimizing the device area may minimize the cost of a heat exchanger. However, as the area of a device increases it may be possible to remove the heat exchanger while producing a given heat transfer rate, as shown in Eq. (24)

$$Q = UA\Delta T \tag{24}$$

where Q is the heat transfer rate, U is the overall heat transfer coefficient, A is the heat transfer surface area, and ΔT is the temperature difference between the two streams. As the area of the device increases, a smaller overall heat transfer coefficient can be used to produce a desired heat transfer rate. By adjusting U and varying A, the heat exchanger characteristics can be modeled and an appropriate heat exchanger can be selected based on the quantity UA. Calculations can be performed to determine when natural convection is adequate to produce a desired heat transfer rate, but these equations are dependent on the orientation of the device in space. By incorporating heat exchanger and substrate costs, a designer can get more information on the overall system cost of a TEC. The formal problem statements to minimize the capital cost (defined in Eq. (19)) are given by Eq. (25).

$$\begin{aligned} \text{Minimize:}\quad & f = C_{\text{capital}} \\ \text{Subject to:}\quad & Q_C - 1.05y \le 0 \\ & 0.95y - Q_C \le 0 \\ & \text{Side bounds established for each architecture} \end{aligned} \tag{25}$$

Further, low efficiency of TECs has limited their adoption to only niche applications. To improve the efficiency of a device and achieve lower long-term costs, a designer may wish to minimize the operating cost of a TEC. To reach a lower operating cost, the device must have a large COP. However, this may sacrifice the capital cost of the device by increasing the complexity of the heat exchanger or inflating the size of the TEC. The formal problem statement to minimize the operating cost of a TEC for a defined Q_C is given in Eq. (26). Once again, Q_C is maintained within ± 5% of a target Q_C value (y). Additionally, various constraints, designated by the value z, on the cross-sectional area of the device (A_{total}) are explored.

$$\begin{aligned} \text{Minimize:}\quad & f = C_{\text{operating}} \\ \text{Subject to:}\quad & Q_C - 1.05y \le 0 \\ & 0.95y - Q_C \le 0 \\ & A_{\text{total}} - z \le 0 \\ & \text{Side bounds established for each architecture} \end{aligned} \tag{26}$$

6 Results

6.1 Multiobjective Optimization.

Pareto frontiers were generated according to the problem statements given in Eq. (22), and the Pareto-optimal solutions are shown in Fig. 4. The hybrid device solutions achieve under 300 W of cooling capacity. This is due to the difference in geometry architecture and the lower ZT

Table 2 Upper and lower bounds on design variables used in optimization problem formulation

Design variable	Bulk architecture		Hybrid architecture	
	Lower bound	Upper bound	Lower bound	Upper bound
Thickness of the TE leg (t)	0.5 mm	0.8 mm	50 μm	250 μm
Width of the TE leg (w)	0.5 mm	0.8 mm	10 mm	20 mm
Length of the TE leg (L)	0.1 mm	1 mm	10 mm	20 mm
Space between the legs (δ)	0.1 mm	2 mm	0.1 mm	2 mm
Input current (I)	0.1 A	10 A	0.1 A	10 A
p-type material (material$_{p\text{-type}}$) (integer)	1	25	26	27
n-type material (material$_{n\text{-type}}$) (integer)	1	25	26	27
Number of thermocouples (N)	1	10,000	1	10,000
Overall heat transfer coefficient (U)	0	100	0	100

values of TE materials available for printing on the PET substrate. Initial expectations were that the hybrid device would be most effective in low density cooling applications. As shown by the colorbar, the hybrid device produces cooling densities lower than the bulk device. The bulk device achieves a heat flux exceeding 14,000 W/m^2 while the hybrid device remains below 2000 W/m^2.

To identify the potential of the hybrid architecture if the efficiency of printable technologies improved, a frontier for the hybrid device using BiSbTe nanobulk is shown in Fig. 5. While using BiSbTe on the hybrid device greatly improves performance, the heat flux is still much lower than the bulk device. The median cooling capacity per area (Q_C/A) for all the hybrid architecture designs is 1808.6 W/m^2; in contrast, the median value for the bulk architecture is 10,011.1 W/m^2. For comparison, the heat flux of R134a direct expansion evaporator coils used in air conditioning and refrigeration can range from 6000 to 8500 W/m^2, and an Energy Star rated central air conditioning unit must have a COP greater than 3.22—translating to an operating cost of \$0.0321/kWh [44]. The use of TECs in high heat flux ($>$100,000 W/m^2) applications is being explored, but current designs have COPs less than 1 (operating costs would be greater than \$0.1035/kWh) [45]. Further, a standard compact refrigerator produces 30–45 W of cooling, and a window unit air conditioner outputs approximately 1500 W of cooling capacity [46,47].

The plots in Figs. 6 and 7 show how individual design variables change as the frontier is traversed. Each solution for the bulk architecture uses BiSbTe nanobulk. These results are in line with Ref. [8], which demonstrated the BiSbTe nanobulk performs well on a \$/kWh basis because of its nanoscale grain structures. For the hybrid architecture, each used the PEDOT material. When calculating ZT per dollar for each material, both PEDOT and BiSbTe nanobulk have the highest efficiency per dollar for their respective architecture.

Another important observation is differences between the overall heat transfer coefficient (U) for both architectures. Since the areas of the hybrid devices are very large, a heat exchanger with a lower heat transfer coefficient can be used to produce a cooling rate across the exchanger, and the heat exchanger component can be greatly simplified. The last observation noted is the optimal current input. As cooling density increases across the Pareto frontier (i.e., more cooling per unit area), the input current increases. A larger current linearly increases the heat pumping capacity of the cooler, but if too large, Joule heating, which is dependent on I^2, can reverse the cooling effects of the device.

For both architectures the solutions make the TE legs as wide as possible, pushing toward the upper bound on thickness (t) and width (w). An important factor in the design of a TEC is the ratio of leg cross-sectional area to leg length. For the bulk architecture, leg area stays constant while the length changes to alter the ratio between the two. This ratio changes between 0.8 and 1.6. A larger ratio translates to increased thermal and electrical conductivity, and a smaller ratio means decreased thermal and electrical conductivity. A large thermal conductivity limits the devices ability to maintain a temperature difference, and a large electrical conductivity lessens the effects of Joule heating.

However, this outcome is not observed for the hybrid architecture, where the leg length remains at the lower bound. When leg area is maximized for the hybrid, but leg length is at its minimum, the largest possible ratio is 0.5. To produce more cooling, a larger ratio is required, but the hybrid architecture is limited by the bounds on the leg thickness, width, and length design variables. Further study and prototyping of a device are needed to test the manufacturing limits of these variables and to assess improvements in design. Initial numerical simulations and experimental results can also be found in Refs. [7] and [49].

To realize how hypothetical improvements in the TE material ZT value could improve performance, additional optimizations were run. Table 4 shows the material properties of BiTe (common in commercially available TECs), BiSbTe nanobulk, and modified versions of BiSbTe nanobulk if each property was improved (e.g., increase α by 10% and decrease κ by 10%) without any additional cost. The results of these optimizations are shown in Fig. 8.

These results indicate the potential of TE material technology. COP increases with improvements in ZT value. This also corresponds to an improvement in operating costs. As ZT of the improved material approaches 3.12, COP values of the TEC reach 3.14, which is more comparable to traditional methods of refrigeration. As a reference, an Energy Star rated central air conditioning unit must have a COP greater than 3.22 [44]. Table 5 provides the minimum, maximum, and median values from the Pareto-optimal solutions.

Table 3 Device properties and operating parameters used in analysis

Property	Value	Reference
T_∞	20 °C	—
T_C	0 °C	—
C''_{bulk}	\$168.23/m^2	[8]
C''_{hybrid}	\$4.76/m^2	[8]
C_{HX}	\$7.60/(W/K)	[8]
C_e	\$0.1035/kWh	[38]
$C_{s,\text{bulk}}$	\$0.8625/m^2	[35]
$C_{s,\text{hybrid}}$	\$0.3985/m^2	[39]
C_{HX}	\$7.60/(W/K)	[8]
$d_{s,\text{bulk}}$	0.5 mm	[2]
$d_{s,\text{hybrid}}$	125 μm	—
$k_{s,\text{bulk}}$	30 W m^{-1} K^{-1}	[40]
$k_{s,\text{hybrid}}$	0.15 W m^{-1} K^{-1}	[41]
R	3% annually	[8]

6.2 Minimize Device Area for a Given Cooling Capacity. The formulation of this optimization problem is given in Eq. (23), where the goal is to minimize the cross-sectional area

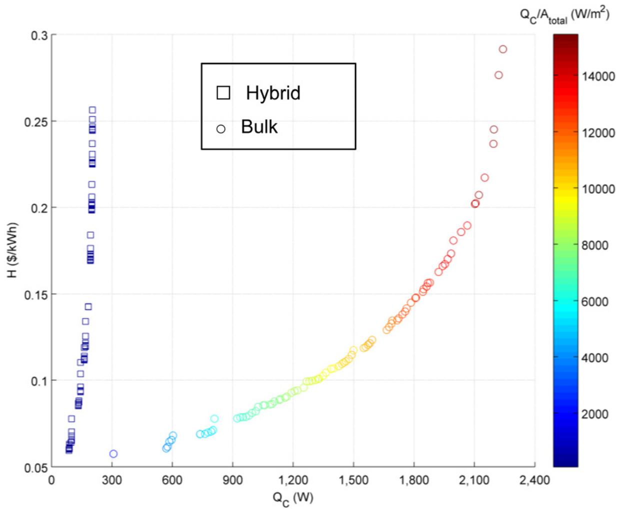

Fig. 4 Pareto frontiers for maximum cooling capacity and minimum cost

of the device (A_{total}) while achieving a target cooling capacity (Q_C). In intervals of 10 W for Q_C values ranging from 10 W to 1000 W, a GA is used. The results for the bulk and hybrid architectures are shown in Fig. 9. The GA evaluated approximately 4600 designs each run.

The hybrid architecture requires a larger area but the number of thermocouples (N) needed is only ten times more. N follows a general linear trend as the amount of cooling and device area increases, translating into a larger area to produce cooling capacity. This is due to the bounds on the design variables from manufacturing considerations and material efficiencies. As defined by the side constraints, the largest possible area for a bulk leg is 0.64 mm^2 (0.8 mm thick by 0.8 mm wide) opposed to 5 mm^2 (0.25 mm thick by 20 mm wide) for a hybrid leg. When including the maximum allowable spacing between the legs, one thermocouple in the bulk architecture has a cross-sectional area up to 15.68 mm^2, and the hybrid architecture has a cross-sectional area up to 99 mm^2.

Additionally, the ZT of PEDOT:PSS material for the hybrid is only 0.26, while the BiSbTe nanobulk used in the bulk has a ZT of 1.68. This requires a larger area to produce cooling in the hybrid architecture. This may prove advantageous in applications where a large heat transfer area is beneficial. An example is personalized cooling and heating, such as an office chair. In these low heat flux uses, localized spot cooling is not needed.

6.3 Minimize Capital Cost. Figure 10 shows the minimum capital costs and the corresponding operating cost, number of thermocouples, and heat exchanger characteristics. Consistent with previous results, the hybrid requires more thermocouples and

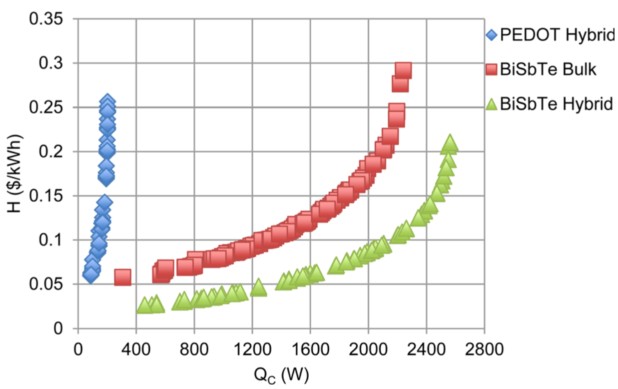

Fig. 5 Pareto frontier using bulk materials for the hybrid architecture

a larger area to produce a desired cooling capacity. The overall heat transfer coefficients for the hybrid architecture are low enough that natural convection can be used to dissipate heat on the hot side of the device, meaning no heat exchanger is necessary. The operating costs are congruent to typical COP values observed in the literature. The range of COP values is 0.296–0.713 for the bulk architecture and 0.074–0.855 for the hybrid architecture.

Figure 11 gives the breakdown of the capital cost for both architectures. For the bulk design, heat exchanger costs average 37.2% of the total cost. In contrast, the heat exchanger costs for the hybrid architecture average 5.4% of the total cost. Calculations can be performed for specific applications to determine if the heat exchanger is required or if natural convection is adequate. Additionally, material cost constituted a large percentage of the hybrid architecture cost. While PEDOT:PSS is an inexpensive material and is easily manufactured via rotary screen printing and R2R processing, the number of thermocouples and volume of material required to produce large cooling capacities limit the economic benefits. Finally, for both architectures, the substrate costs were a small component of the total costs.

Due to the large area of PET substrate required for the hybrid device, a greater cost is contributed by the hybrid substrate than the bulk substrate. The consequences of these insights help to identify potential areas where the TEC systems can be improved. While the materials comprising the hybrid are inexpensive, the large volume of materials used limits cost savings. These initial results suggest that at very low Q_c values (less than 110 W), the hybrid architecture may be the best solution to adopt. For Q_c values around 400 W, more detailed analysis may be needed to understand the cost associated with heat exchanger design to determine if the bulk architecture is truly a more cost effective strategy. However, these results suggest that at large values of Q_C, the bulk architecture is more cost effective, even with the cost associated with heat exchanger design.

6.4 Minimize Operating Cost. Opposed to minimizing the capital costs of a TEC, a designer may wish to minimize the operating cost to reduce the lifetime expense of the device. Four different constraints on A_{total} are examined: 500,000 mm^2, 250,000 mm^2, 125,000 mm^2, and 62,500 mm^2. The results are shown in Fig. 12. Bulk architecture solutions range in area from 3421 mm^2 to 60,004 mm^2. When unconstrained, operating costs are reduced to under \$0.06/hr at 1000 W of cooling. This sharply contrasts to operating costs as large as \$0.30/hr when minimizing for capital cost.

Table 6 gives the maximum and minimum COPs found for each scenario. The minimum COP corresponds to the maximum cooling capacity, while the maximum COP corresponds to the minimum cooling capacity. As the constraint on area is approached, the cooling capacity output decreases and the operating costs of the hybrid rapidly increase. This creates a sharp rise in operating cost. When area is unconstrained, the hybrid is competitive with the bulk architecture. As shown in Secs. 6.2 and 6.3, the area of the bulk device is minimal compared to the hybrid device; as a result, the operating cost of a bulk TEC is unaffected by the constraints explored here. Additionally, to minimize capital costs, the heat exchanger is greatly simplified as it can be a major component of the overall system cost. When minimizing for operating costs, the overall heat transfer coefficient grows to increase the cooling transfer efficiency.

7 Conclusions and Future Work

This paper explores the performance and design spaces of a bulk and hybrid TEC architecture. Multiple optimizations were used to explore the transition from theoretical development to real-world application. Each optimization offers insight into TEC design, and the cost analysis provides a lower bound on the expected capital and operating costs.

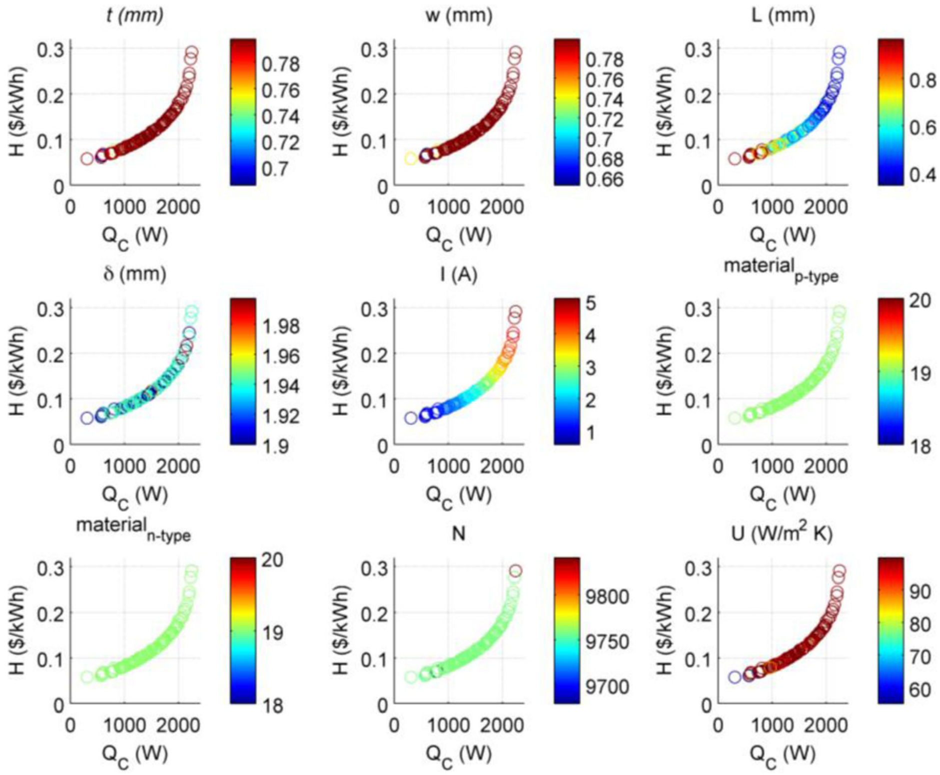

Fig. 6 Design variable trends for bulk architecture (color bar represents variable value)

The results of the multiobjective optimization demonstrated the tradeoff between cost and device performance. In different regions of the performance space, one architecture or material choice may be a more effective solution. At high heat flux requirements, the bulk device with BiSbTe nanobulk material is the most effective option. At lower heat flux requirements, both hybrid and bulk solutions are found. However, TECs with current technologies still lag behind traditional methods when considering efficiency. Developing materials with increased ZT (to around 3) will yield COP values close to the Energy Star standard for central air conditioning [44]. With continued material advancements, the economic and cooling performance viability of TECs as an

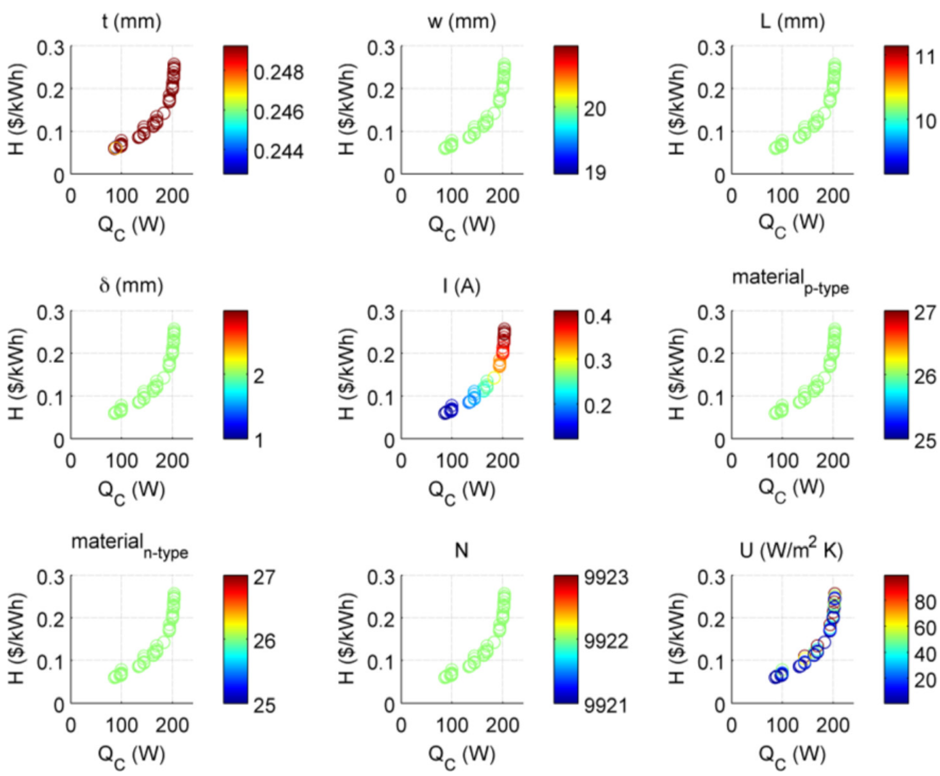

Fig. 7 Design variable trends for hybrid architecture (color bar represents variable value)

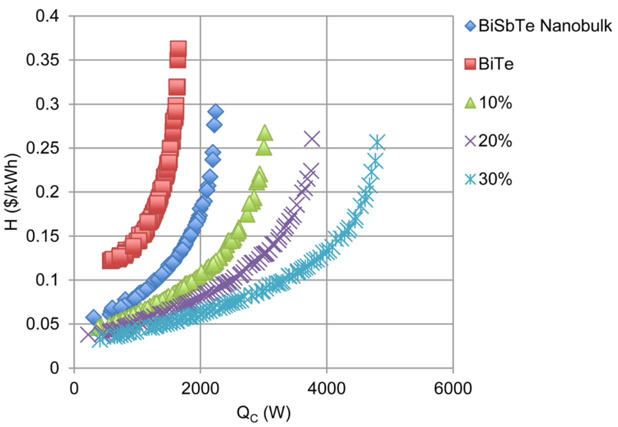

Fig. 8 Pareto frontiers for improved hypothetical TE materials in a bulk TEC

Table 4 Improved material properties for analysis

Material	α (V/K)	ρ (Ω mm)	κ (W/mm K)	ZT (300 K)
BiTe	0.000227	0.011475	0.00157	0.858
BiSbTe nanobulk	0.000224	0.013177	0.00068	1.680
10% improvement	0.000246	0.014495	0.00061	2.053
20% improvement	0.000269	0.015812	0.00054	2.520
30% improvement	0.000291	0.017130	0.00048	3.120

alternative to traditional cooling methods grows. Yet, the hybrid architecture may not be as attractive as a bulk device even in low heat flux applications. If printable TE materials can be improved to attain ZT values similar to those available for bulk devices, the hybrid architecture becomes a more attractive solution.

Table 5 COP results for Pareto-optimal solutions

Material	Minimum COP	Maximum COP	Median COP
BiTe	0.276	0.826	0.567
BiSbTe nanobulk	0.343	1.762	0.927
10% improvement	0.374	2.203	1.133
20% improvement	0.384	2.656	1.252
30% improvement	0.390	3.141	1.261

As demonstrated in the literature, maximizing leg area while decreasing leg length yields increased cooling capacities. BiSbTe nanobulk material is a promising alternative to the conventional BiTe modules currently on the market. As heat flux increases (i.e., more cooling per unit area), the input current increases; as a result, the optimal current for the hybrid architecture was much lower than that for the bulk architecture. Additionally, since the areas of the hybrid devices are very large, a heat exchanger with a lower heat transfer coefficient can be used to produce a cooling rate across the exchanger.

TECs with current technologies still lag behind traditional methods when considering efficiency. Future improvements in TE technology could ease these limitations, and cost information could offer insight into potential areas to investigate. As the thermoelectric figure of merit (ZT) of a material increases, this directly translates into an increased COP and reduced operating costs.

A majority of the total device cost is associated with operating cost, so consideration of the material efficiency and device COP is integral in the design of a TEC. These trends are similar in both the hybrid and bulk architectures. Capital cost, however, is still an important factor. Heat exchangers are a large component of the TEC capital cost, particularly for the bulk architecture. Material cost is more expensive for the bulk architecture, but the large area of the hybrid architecture leads to a larger volume of material and substrate. In addition, the inexpensive polymer hybrid device is unable to compete from a performance standpoint with bulk

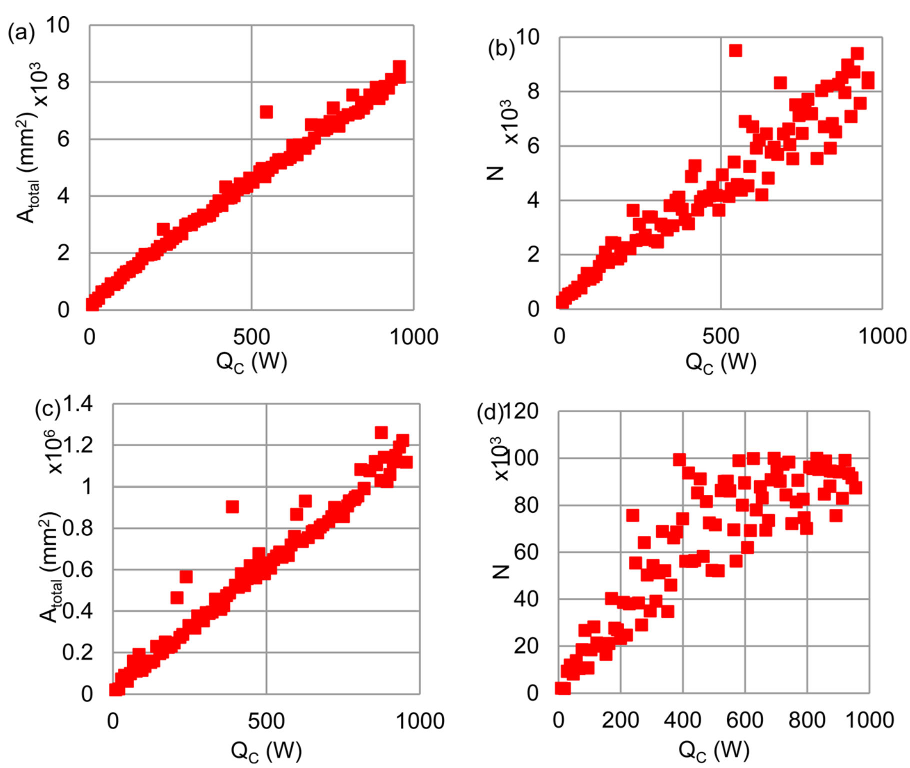

Fig. 9 (*a*) Minimum cross-sectional area to produce a given Q_C and (*b*) corresponding number of thermocouples of the bulk architecture, and (*c*) minimum cross-sectional area to produce a given Q_C and (*d*) corresponding number of thermocouples of the hybrid architecture

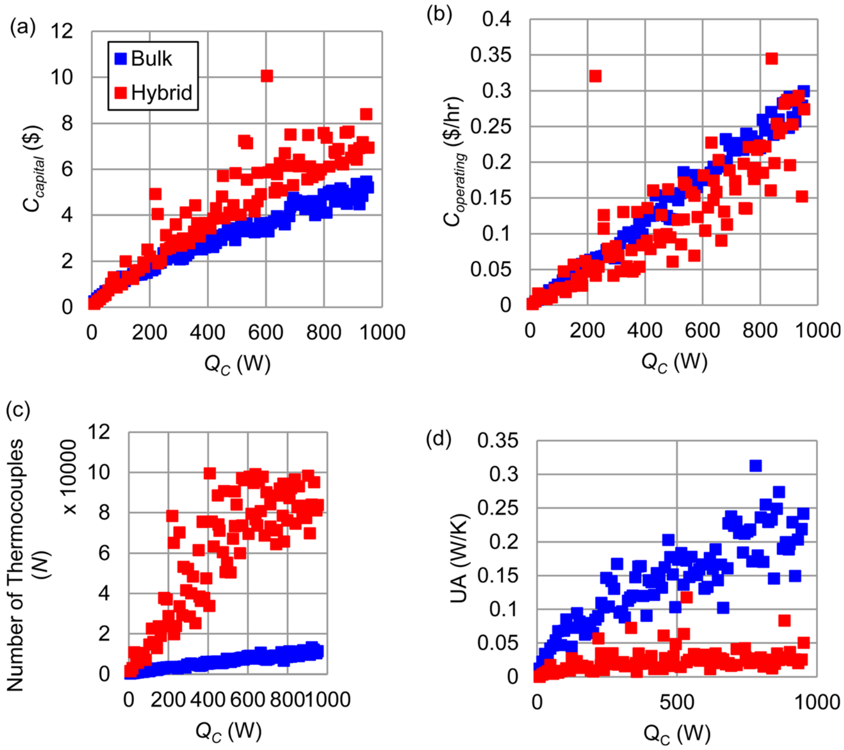

Fig. 10 (*a*) **Minimal capital cost at a given** Q_C **for bulk and hybrid architectures, (*b*) the operating cost, (*c*) the number of thermocouples, and (*d*) the heat exchanger characteristic**

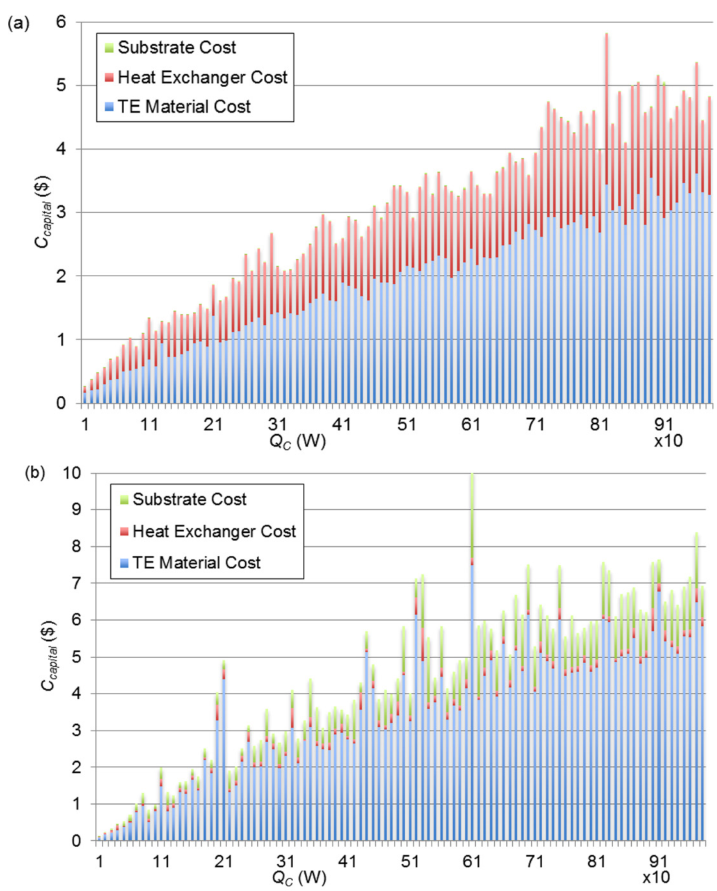

Fig. 11 Breakdown of capital cost for (*a*) bulk and (*b*) hybrid architectures

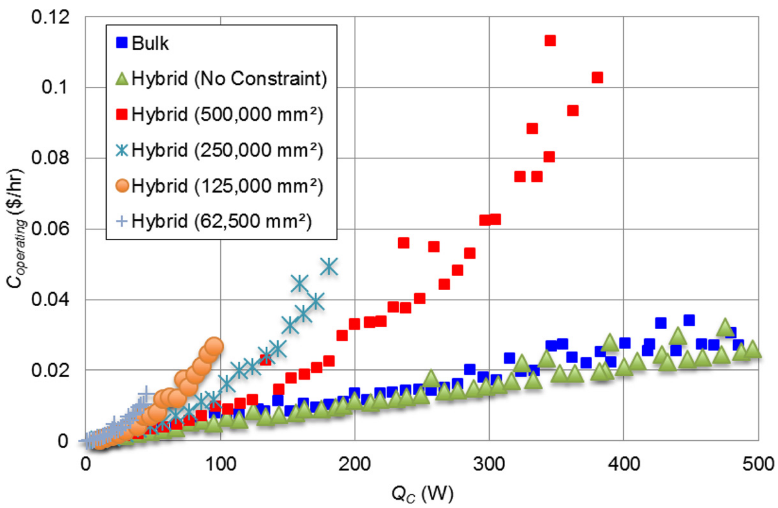

Fig. 12 Minimized operating cost under different cross-sectional area constraints

Table 6 Minimum and maximum COP of bulk and hybrid TECs under device area constraints

	Bulk		Hybrid	
Constraint	Min COP	Max COP	Min COP	Max COP
Unconstrained	1.242	1.791	1.126	1.932
500,000 mm ^{2}	—	—	0.305	1.908
250,000 mm ^{2}	—	—	0.356	1.827
125,000 mm ^{2}	—	—	0.352	1.810
62,500 mm ^{2}	—	—	0.335	1.891

devices and materials with higher ZT values. Consequently, the substrate and TE material are large components of the hybrid device's overall system cost, and even through the material is inexpensive, a sacrifice in performance exists to create deficiencies when compared to the bulk device. Increased research is needed to more accurately compare the costs associated with manufacturing for each architecture. At high levels of Q_C, it is likely that the bulk architecture is the dominant design. However, as the targeted value of Q_C decreases, manufacturing costs can play a significant role, especially as the size of each device increases. Further, there may be application-specific requirements that require the design of the hybrid architecture—it must be distributed over a wide area—that would make the costs of designing a similarly scaled bulk architecture prohibitive.

By identifying these major cost components, opportunities for savings and improvements are indicated. Future work includes an analysis of additional device architectures, including thin-film devices and a hybrid architecture with a sinusoidal structure. The authors have conducted initial experiments with these architectures to validate the analysis presented in this paper [7,49]. It is evident that manufacturing constraints are limiting the performance of both the bulk and hybrid architectures and that certain costs of heat exchanger, substrate, or material are prohibiting factors. While advancements in materials and manufacturing techniques are outside the scope of this research, further exploration of the limitations placed on the device architectures by currently available technology and of the available options for heat exchanger optimization is warranted. A detailed cost metric that comprehensively models the R2R manufacturing process for hybrid devices and the production of bulk TECs could contribute to a more complete understanding of these limitations. In addition, both R2R processing and device prototypes would provide further insights into the cost and cooling performance of the device architectures.

Acknowledgment

The authors gratefully thank the Eastman Chemical Company for the financial support of this work.

Nomenclature

a, b = conversion factors from rectangular to circular geometry
A = cross-sectional area
Bi = Biot number
C = cost
C'' = areal material cost
C''' = volumetric material cost
COP = coefficient of performance
d_s = substrate thickness
I = input current
K = thermal conductance
L = TE leg length
N = number of thermocouples
P = input power
Q = cooling/heating capacity
R = electrical conductivity
R = amortization rate
t = TE leg thickness
T = absolute temperature
TEC = thermoelectric cooler
TEG = thermoelectric generator
U = overall heat transfer coefficient
w = TE leg width
ZT = thermoelectric material figure of merit

Greek Symbols

α = Seebeck coefficient
δ = space between the legs
ε = contact radius
κ = thermal conductivity
λ_c = empirical parameter
ρ = electrical resistivity
τ = plate thickness
ψ = dimensionless spreading resistance

Subscripts

C = cold side
H = hot side
HX = heat exchanger
n = n-type material
p = p-type material
s = substrate
TE = thermoelectric material

Appendix

Table 7 Thermoelectric material properties and cost

Material	Type	α (V/K)	ρ (Ω mm)	κ (W/mm K)	C''' (\$/mm^3)	C'' (\$/mm^2)	No.	Reference
Bulk material selection								
Bi_2Te_3	Bulk	−0.000227	0.011474864	0.00157	0.000889565	0.00016823	1	[29]
$Bi_{0.52}Sb_{1.48}Te_3$	Bulk	0.000202	0.007702973	0.00141	0.000865743	0.00016823	2	[29]
$AgPb_{18}SbTe_{20}$	Bulk	−0.000121	0.005076142	0.00228	0.00077717	0.00016823	3	[29]
SiGe	Bulk	0.000117	0.01075963	0.00495	0.003044917	0.00016823	4	[29]
$Mg_2Si_{0.6}Sn_{0.4}$	Bulk	−0.000089	0.00513901	0.0033	1.68306×10^{-5}	0.00016823	5	[29]
$MnSi_{1.75}$	Bulk	0.000183	0.127129418	0.00234	7.33212×10^{-6}	0.00016823	6	[29]
$Ba_8Ga_{16}Ge_{28}Zn_2$	Bulk	−0.00011	0.033696128	0.00139	0.003123358	0.00016823	7	[29]
$Ba_8Ga_{16}Ge_{30}$	Bulk	−0.000035	0.006281802	0.00172	0.003230061	0.00016823	8	[29]
$Ba_7Sr_1Al_{16}Si_{30}$	Bulk	−0.000023	0.00569833	0.00237	0.000005346	0.00016823	9	[29]
$CeFe_4Sb_{12}$	Bulk	0.000074	0.004444642	0.0026	0.000262299	0.00016823	10	[29]
$Yb_{0.2}In_{0.2}Co_4Sb_{12}$	Bulk	−0.00013	0.006144016	0.00325	0.000193688	0.00016823	11	[29]
$Ca_{0.18}Co_{3.97}Ni_{0.03}Sb_{12.40}$	Bulk	−0.000124	0.005062778	0.00571	9.3016×10^{-5}	0.00016823	12	[29]
$(Zn_{0.98}Al_{0.02})O$	Bulk	−0.000084	0.01173282	0.04073	0.000020128	0.00016823	13	[29]
$Ca_{2.4}Bi_{0.3}Na_{0.3}Co_4O_9$	Bulk	0.000124	0.093826234	0.00201	0.00017294	0.00016823	14	[29]
$Na_{0.7}CoO_{2-\delta}$	Bulk	0.000081	0.003024529	0.01993	0.000195925	0.00016823	15	[29]
$Zr_{0.25}Hf_{0.25}Ti_{0.5}NiSn_{0.994}Sb_{0.006}$	Bulk	−0.000208	0.012187988	0.00286	8.06371×10^{-5}	0.00016823	16	[29]
$Zr_{0.5}Hf_{0.5}Ni_{0.8}Pd_{0.2}Sn_{0.99}Sb_{0.01}$	Bulk	−0.000103	0.004784689	0.00464	9.1203×10^{-5}	0.00016823	17	[29]
$Ti_{0.8}Hf_{0.2}NiSn$	Bulk	−0.000115	0.042971939	0.00405	8.64239×10^{-5}	0.00016823	18	[29]
$Bi_{0.52}Sb_{1.48}Te_3$	Nanobulk	0.000224	0.013176967	0.00068	0.00087975	0.00016823	19	[29]
$(Na_{0.0283}Pb_{0.945}Te_{0.9733})(Ag_{1.11}Te_{0.555})$	Nanobulk	0.000069	0.01140576	0.00171	0.000748177	0.00016823	20	[29]
$Si_{80}Ge_{20}$	Nanobulk	0.000114	0.011866619	0.00246	0.001303838	0.00016823	21	[29]
$Mg_2Si_{0.85}Bi_{0.15}$	Nanobulk	0.000098	0.008305648	0.00752	3.34809×10^{-5}	0.00016823	22	[29]
Si	Nanobulk	−0.000064	0.004816492	0.0128	9.7627×10^{-6}	0.00016823	23	[29]
$Mn_{15}Si_{28}$	Nanobulk	0.000111	0.029804483	0.00275	1.09881×10^{-5}	0.00016823	24	[29]
PEDOT:PSS	Polymer	0.00021	0.135135135	0.00037	0.00000051	0.00000476	25	[3]
Hybrid material selection								
PEDOT:PSS	Polymer	0.00021	0.135135135	0.00037	0.00000051	0.00000476	26	[3]
Bi_2Te_3	Composite	0.0001585	0.1621645	0.00024	0.000865743;	0.00000476	27	[48]

References

[1] Rowe, D. M., 2006, *Thermoelectrics Handbook: Macro to Nano*, CRC/Taylor & Francis, Boca Raton, FL.

[2] Ferrotec, 2014, "Thermal Reference Guide," Last accessed Jan. 26, 2014, https://thermal.ferrotec.com/technology/thermal/thermoelectric-reference-guide

[3] Bell, L. E., 2008, "Cooling, Heating, Generating Power, and Recovering Waste Heat With Thermoelectric Systems," Science, **321**(5895), pp. 1457–1461.

[4] DiSalvo, F. J., 1999, "Thermoelectric Cooling and Power Generation," Science, **285**(5428), pp. 703–706.

[5] Cheng, T.-C., Cheng, C.-H., Huang, Z.-Z., and Liao, G.-C., 2011, "Development of an Energy-Saving Module Via Combination of Solar Cells and Thermoelectric Coolers for Green Building Applications," Energy, **36**(1), pp. 133–140.

[6] Sun, T., Peavey, J. L., Shelby, M. D., Ferguson, S., and O'Connor, B. T., 2015, "Heat Shrink Formation of a Corrugated Thin Film Thermoelectric Generator," Energy Convers. Manage., **103**, pp. 674–680.

[7] Owoyele, O., Ferguson, S., and O'Connor, B. T., 2015, "Performance Analysis of a Thermoelectric Cooler With a Corrugated Architecture," Appl. Energy, **147**, pp. 184–191.

[8] LeBlanc, S., Yee, S. K., Scullin, M. L., Dames, C., and Goodson, K. E., 2014, "Material and Manufacturing Cost Considerations for Thermoelectrics," Renewable Sustainable Energy Rev., **32**, pp. 313–327.

[9] Song, S., Au, V., and Moran, K. P., 1995, "Constriction/Spreading Resistance Model for Electronics Packaging," 4th ASME/JSME Thermal Engineering Joint Conference, Vol. 4, pp. 199–206.

[10] Yazawa, K., and Shakouri, A., 2012, "Scalable Cost/Performance Analysis for Thermoelectric Waste Heat Recovery Systems," J. Electron. Mater., **41**(6), pp. 1845–1850.

[11] Chen, G., Dresselhaus, M. S., Dresselhaus, G., Fleurial, J.-P., and Caillat, T., 2003, "Recent Developments in Thermoelectric Materials," Int. Mater. Rev., **48**(1), pp. 45–66.

[12] Snyder, G. J., and Toberer, E. S., 2008, "Complex Thermoelectric Materials," Nat. Mater., **7**(2), pp. 105–114.

[13] Søndergaard, R. R., Hösel, M., Espinosa, N., Jørgensen, M., and Krebs, F. C., 2013, "Practical Evaluation of Organic Polymer Thermoelectrics by Large-Area R2R Processing on Flexible Substrates," Energy Sci. Eng., **1**(2), pp. 81–88.

[14] Bubnova, O., Khan, Z. U., Malti, A., Braun, S., Fahlman, M., Berggren, M., and Crispin, X., 2011, "Optimization of the Thermoelectric Figure of Merit in the Conducting Polymer Poly (3, 4-Ethylenedioxythiophene)," Nat. Mater., **10**(6), pp. 429–433.

[15] Kim, G. H., Shao, L., Zhang, K., and Pipe, K. P., 2013, "Engineered Doping of Organic Semiconductors for Enhanced Thermoelectric Efficiency," Nat. Mater., **12**(8), pp. 719–723.

[16] Yamanashi, M., 1996, "A New Approach to Optimum Design in Thermoelectric Cooling Systems," J. Appl. Phys., **80**(9), pp. 5494–5502.

[17] Huang, B. J., Chin, C. J., and Duang, C. L., 2000, "A Design Method of Thermoelectric Cooler," Int. J. Refrig., **23**(3), pp. 208–218.

[18] Cheng, Y.-H., and Lin, W.-K., 2005, "Geometric Optimization of Thermoelectric Coolers in a Confined Volume Using Genetic Algorithms," Appl. Therm. Eng., **25**(17–18), pp. 2983–2997.

[19] Cheng, Y.-H., and Shih, C., 2006, "Maximizing the Cooling Capacity and COP of Two-Stage Thermoelectric Coolers Through Genetic Algorithm," Appl. Therm. Eng., **26**(8–9), pp. 937–947.

[20] Nain, P. K. S., Giri, J. M., Sharma, S., and Deb, K., 2010, "Multi-Objective Performance Optimization of Thermo-Electric Coolers Using Dimensional Structural Parameters," *Swarm, Evolutionary, and Memetic Computing*, Vol. 6466, B. K. Panigrahi, S. Das, P. N. Suganthan, and S. S. Dash, eds., Springer, Berlin, pp. 607–614.

[21] Zhou, Y., and Yu, J., 2012, "Design Optimization of Thermoelectric Cooling Systems for Applications in Electronic Devices," Int. J. Refrig., **35**(4), pp. 1139–1144.

[22] Huang, Y.-X., Wang, X.-D., Cheng, C.-H., and Lin, D. T.-W., 2013, "Geometry Optimization of Thermoelectric Coolers Using Simplified Conjugate-Gradient Method," Energy, **59**, pp. 689–697.

[23] Venkata Rao, R., and Patel, V., 2013, "Multi-Objective Optimization of Two Stage Thermoelectric Cooler Using a Modified Teaching–Learning-Based Optimization Algorithm," Eng. Appl. Artif. Intell., **26**(1), pp. 430–445.
[24] Khanh, D. V. K., Vasant, P., Elamvazuthi, I., and Dieu, V. N., 2014, "Optimization of Thermo-Electric Coolers Using Hybrid Genetic Algorithm and Simulated Annealing," Arch. Control Sci., **24**(2), pp. 155–176.
[25] Yee, S. K., LeBlanc, S., Goodson, K. E., and Dames, C., 2013, "A $/W Metric for Thermoelectric Power Generation: Beyond ZT," Energy Environ. Sci., **6**(9), pp. 2561–2571.
[26] Kim, H., and Kim, W., 2015, "A Way of Achieving a Low $/W and a Decent Power Output From a Thermoelectric Device," Appl. Energy, **139**(2), pp. 205–211.
[27] SPGPrints, 2015, *RotaMesh Specifications*, SPGPrints, Boxmeer, The Netherlands.
[28] Yates, P., 2014, "Quote Request," Last accessed Nov. 12, **2014**, http://www.spgprints.com/
[29] Chen, A., Madan, D., Wright, P. K., and Evans, J. W., 2011, "Dispenser-Printed Planar Thick-Film Thermoelectric Energy Generators," J. Micromech. Microeng., **21**(10), p. 104006.
[30] Søndergaard, R. R., Hösel, M., and Krebs, F. C., 2013, "Roll-to-Roll Fabrication of Large Area Functional Organic Materials," J. Polym. Sci., Part B, **51**(1), pp. 16–34.
[31] Lee, H., 2013, "The Thomson Effect and the Ideal Equation on Thermoelectric Coolers," Energy, **56**, pp. 61–69.
[32] Goldsmid, H. J., 2009, *Introduction to Thermoelectricity*, Springer-Verlag, Berlin.
[33] Shah, R. K., and Sekulic, D. P., 2003, *Fundamentals of Heat Exchanger Design*, Wiley, Hoboken, NJ.
[34] Matthews, L. M., 1983, *Estimating Manufacturing Costs: A Practical Guide for Managers and Estimators*, McGraw-Hill, New York.
[35] National Minerals Information Center, *Minerals Statistics and Information from the USGS*, U.S. Department of the Interior, U.S. Geological Survey.
[36] Pareto, V., 1971, *Manual of Political Economy*, A. M. Kelley, New York.
[37] Salleo, A., and Wong, W. S., 2009, *Flexible Electronics: Materials and Applications*, Springer, New York.
[38] Hankey, R., Cassar, C., Peterson, R., Wong, P., and Knaub, J., Jr., 2014, *Electric Power Monthly With Data for October 2014*, U.S. Department of Energy, Washington, DC.
[39] Esposito, F., "Resin Pricing," Last accessed Jan. 12, 2015, http://www.plasticsnews.com/resin/engineering-thermoplastics/current-pricing
[40] Auerkari, P., 1996, *Mechanical and Physical Properties of Engineering Alumina Ceramics*, Technical Research Center of Finland, VTT.
[41] Speight, J., 2004, *Lange's Handbook of Chemistry*, 70th Anniversary Edition, McGraw-Hill, New York.
[42] Deb, K., Pratap, A., Agarwal, S., and Meyarivan, T., 2002, "A Fast and Elitist Multiobjective Genetic Algorithm: NSGA-II," IEEE Trans. Evol. Comput., **6**(2), pp. 182–197.
[43] MathWorks, 2004, *Global Optimization Toolbox: User's Guide (R2013b)*, The MathWorks, Natick, MA.
[44] "Air-Source Heat Pumps and Central Air Conditioners Key Product Criteria," Last accessed Jan. 19, 2015, https://www.energystar.gov
[45] Ranjan, R., Turney, J. E., Lents, C. E., and Faustino, V. H., 2014, "Design of Thermoelectric Modules for High Heat Flux Cooling," ASME J. Electron. Packag., **136**(4), p. 041001.
[46] "LW1511ER Specification sheet," LG Electronics U.S.A., Inc., Englewood Cliffs, NJ.
[47] "Frigidaire 2.4 Cu. Ft. Compact Refrigerator Black—FFPE2411QB," Last accessed Mar. 9, 2015, http://www.frigidaire.com/Kitchen-Appliances/Refrigerators/Compact-Refrigerator/FFPE2411QB
[48] "Standard Modules," TE Technology, Last accessed Feb. 21, 2015, https://tetech.com/peltier-thermoelectric-cooler-modules/standard/
[49] Tianlei, S., Peavey, J., Shelby, M., Ferguson, S., and O'Connor, B., 2015, "Heat Shrink Formation of a Corrugated Thin Film Thermoelectric Generator," J. Energy Convers. Manage., **103**, pp. 674–680.